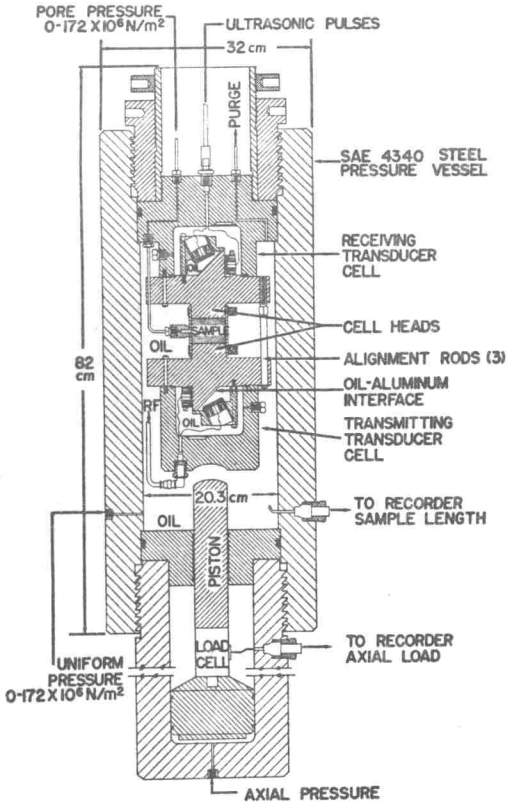

Fig. 6. Dual-mode ultrasonic apparatus assembled for triaxial loading of sample.

directly through the neoprene sleeve. The apparatus is designed for independent control of both external and pore pressures between 0 and 25 000 lbf/in^2 (172 $\times$ 10^6 N/m^2). Total axial loads up to 50 000 lbf/in^2 (344 $\times$ 10^6 N/m^2) can be achieved. The designed pressure limits of the apparatus exceed those required to restore subsurface stress conditions on cores recovered from the deepest existing well bores, i.e., about 7800 meters.

Coupling aids between the heads of the transducer cells and the sample are sometimes required for propagation of S waves. A small amount of Permatex nonhardening form-a-gasket compound placed on the ends of the sample is useful as a coupling medium. A layer of lead foil having an initial thickness of 0.025 mm has also been used successfully. A linear motion potentiometer is mounted parallel with the sample between the cells. The device measures to the nearest 0.025 mm and detects changes in sample length caused by the loading.

Electronic-Acoustic System

Fig. 7 shows the electronic system associated with the ultrasonic apparatus. The output of the oscillator is switched on and off by a tone-burst generator to form phase-coherent repetitive RF pulses. The RF of the pulses matches the resonant frequency of the piezoelectric transducers. Normally, the pulse length is 5 to 8 cycles and the interval between pulses is 10 to 20 ms. These pulses are amplified to 50–120 volts p/p and applied alternately through a coaxial relay switch to the P-wave and S-wave emitter transducers, which in turn generate

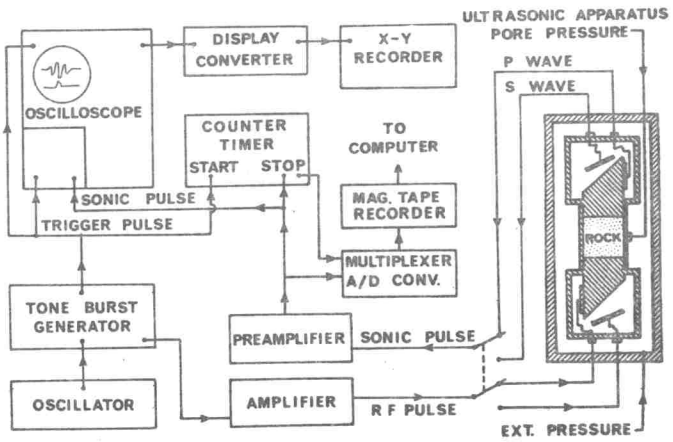

Fig. 7. Schematic diagram of electronic-acoustic system.

ultrasonic pulses. After passing through the sample and receiving transducer, these pulses are amplified and displayed by the oscilloscope.

The trigger pulse from the tone-burst generator coincides with the origin of the transmitted RF pulse. This trigger pulse not only opens the gate of the counter–timer and synchronizes the delayed sweep of the oscilloscope, but also provides a stable reference signal which is independent of the amplitude of the transmitted RF pulse. The received ultrasonic pulses close the gate of the counter at the desired reference cycle. The display converter permits x–y recording of signals that appear on the deflection electrodes of the oscilloscope. Transit times and analog signals representing output waveforms of both P waves and S waves are digitized and recorded on magnetic tape for computer processing.

Calibration of Apparatus

The apparatus is calibrated in the pressure vessel with the heads of the transducer cells placed face to face with no sample between them. Travel times ΔT_p and ΔT_s of P-wave and S-wave pulses (Fig. 8) are measured at various pressure levels. To account for small differences in travel time caused by the loading, the apparatus must be calibrated under actual operating conditions. Observed changes in ΔT_p and ΔT_s were found to be reproducible and amounted to less than 0.1 μs in the pressure range 0 to 70 $\times$ 10^6 N/m^2. Subsequent travel times measured with a sample between the transducer cells at a given pressure level were corrected by subtracting the travel times obtained by calibration at the corresponding pressure level.

Measurement of Transit Times

Fig. 9 shows typical P-wave pulses obtained with and without a sample of Solenhofen limestone between the heads of the transducer cells. Calibrated marker outputs from the counter–timer were manually adjusted to indicate visually the exact parts of the waveforms that are being used to start and stop the counter. The leading edges of the markers have rise times of 2 ns. The travel time of the P wave through the rock is the difference

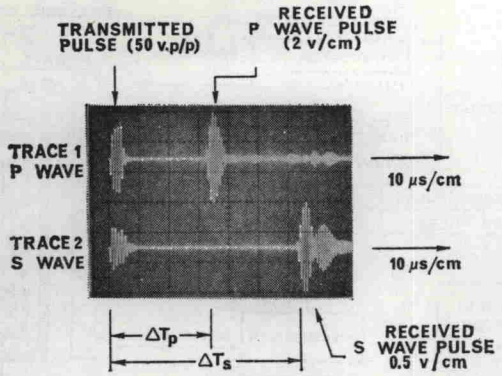

Fig. 8. *P*-wave and *S*-wave pulses obtained through dual-mode apparatus with cell heads placed face to face (no sample).

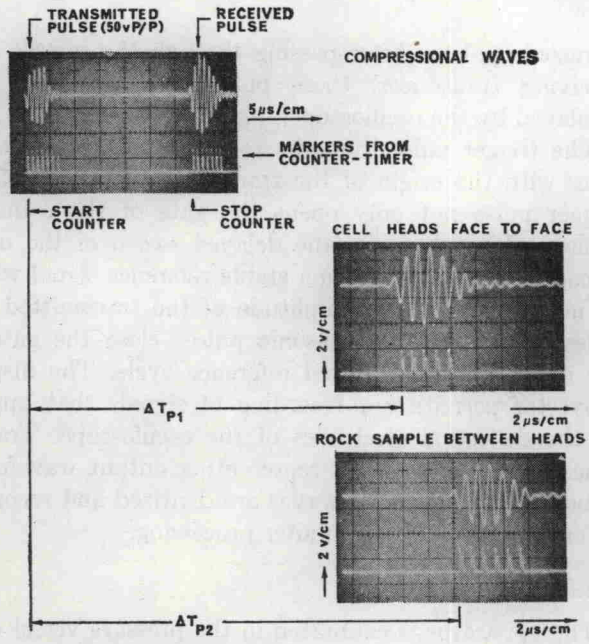

Fig. 9. Measurement of *P*-wave pulse travel time through sample of Solenhofen limestone.

between ΔT_{p2} and ΔT_{p1} and is determined to a resolution of 10^{-2} μs.

Similarly, the travel time of the *S*-wave pulse through the same rock sample is determined by the difference between ΔT_{s2} and ΔT_{s1} as shown in Fig. 10. Measured travel times ΔT_{p1} and ΔT_{s1} agree well with those computed using the known velocities and lengths in aluminum and oil between the transmitting and receiving transducers. These illustrations indicate that the count is started by the first negative peak of the transmitted pulse. In practice, the trigger pulse, which coincides with the start of the transmitted pulse, starts the count as shown in Fig. 7.

Certain types of geological material may cause the carrier frequency of the tone-burst pulse to be highly attenuated. Changes in pulse shape may indicate dispersion caused by inhomogeneities in the sample. If serious absorption or dispersion occurs, the accuracy of travel times measured with a tone-burst pulse is in peril. For these troublesome materials, a single V-shaped pulse

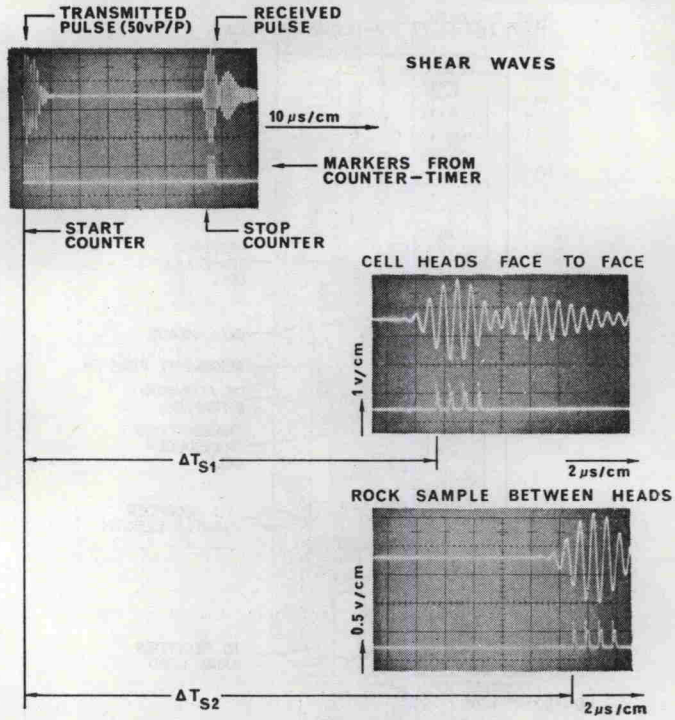

Fig. 10. Measurement of *S*-wave pulse travel time through sample of Solenhofen limestone.

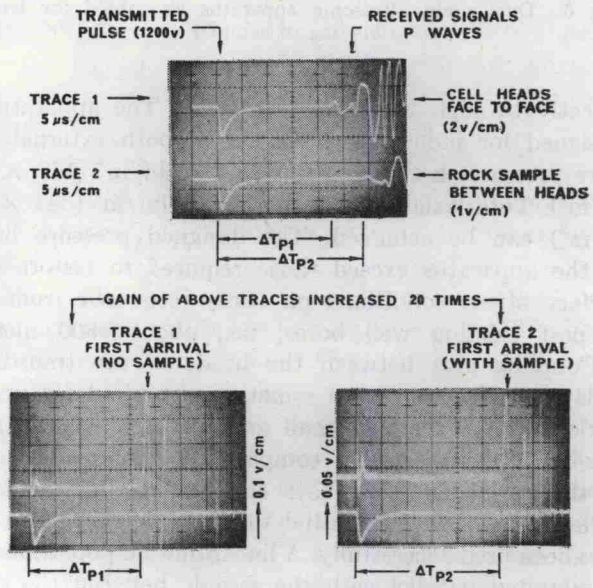

Fig. 11. Measurement of *P*-wave pulse travel time through sample of Solenhofen limestone using single-pulse method.

with a broad frequency spectrum is used for determining both *P*-wave and *S*-wave transit time. Examples of *P*-wave signals are shown in Fig. 11. The *S* waves are similar in appearance but some low-level *P* waves occur as precursors in the wavetrain. The V-shaped excitation pulse imposes 1200 volts on the transmitting transducer, and a strong acoustic signal is obtained through most materials. Transit times are measured between the first negative break of the transmitted pulse and the first positive break in the received signal. Distortion of the received wave train is not important, but the rise time of